FeS2 Nanocrystal Ink as a Catalytic Electrode for Dye-Sensitized Solar Cells**

Ying-Chiao Wang, Di-Yan Wang, You-Ting Jiang, Hsin-An Chen, Chia-Chun Chen, Kuo-Chuan Ho, Hung-Lung Chou, and Chun-Wei Chen**

In the last decade, dye-sensitized solar cells (DSSCs) have attracted great interest for the fabrication of low-cost large-area photovoltaic devices as an alternative to conventional inorganic counterparts.[1–5] The counter electrode (CE) is a critical component in DSSCs, where electrons are injected into the electrolyte to catalyze iodine reductions (I_3^- to I^-).[6] The most commonly used CE is based on indium-doped tin oxide (ITO)-coated glass loaded with platinum by sputtering. Platinum has a high catalytic activity for triiodide reduction and presents sufficient corrosion resistance. However, Pt is expensive because of its scarcity, and thus, the development of so-called Pt-free CEs for DSSCs using cheaper and abundant materials becomes technologically desirable. Recently, carbon-based materials, such as graphite, graphene, carbon nanotubes, and conducting polymers, have been used to replace Pt as electrocatalysts for triiodide reduction in DSSCs,[7–12] although these devices still suffer from poor thermal stability and weak corrosion resistance. Extensive research has been performed on using inorganic compounds such as transitional metal carbides, nitrides, oxides, and sulfides as a new class of alternative catalytic materials for Pt in DSSC systems.[13–20] Therefore, pursuing low-cost and stable

CE materials as alternatives to expensive Pt is crucial to make DSSC systems more competitive for future commercial applications.

Pyrite iron disulfide (FeS2, so-called fool's gold) is an interesting next-generation photovoltaic material candidate that is abundant in nature and is nontoxic. It is ranked as having the highest material availability among 23 existing semiconducting photovoltaic systems[21] that could potentially lead to lower costs compared to conventional silicon solar cells. Colloidal pyrite nanocrystals (NCs) were recently synthesized and characterized,[22–24] providing great potential for developing low-cost fabrications of FeS2-based photovoltaic devices using solution processes. We first demonstrated pyrite NC-based photodiode devices with a spectral response extended to near infrared (NIR) wavelengths because of its large optical absorption coefficient ($> 10^5\ cm^{-1}$) and narrow band gap of 0.95 eV, which provided a crucial step toward success in producing colloidal pyrite NCs thin films as photovoltaic absorption layers.[25] This study demonstrates an important photovoltaic application using FeS2 nanocrystal pyrite ink to fabricate a cost-effective CE in DSSCs, which has the unique advantages of earth abundance and of being solution-processable. The DSSC device with the CE using the FeS2 NC ink exhibits a promising power conversion efficiency of 7.31 % comparable to that of the cell using the precious metal of Pt deposited by sputtering (7.52 %), as well as remarkable electrochemical stability of greater than 500 consecutive cycle scans. Solution-processable and semi-transparent FeS2 NC-based CEs also enable the fabrication of flexible and bifacial DSSCs. The results indicate that FeS2 NC ink is an extremely promising candidate for replacing Pt to substantially reduce the cost of DSSCs in future commercial applications and have also shed light on employing the low-cost FeS2 NC catalyst in other electrochemical cells.

The FeS2 NCs were prepared using wet solution-phase chemical syntheses[26] with a number of modifications according to our previous reports.[22,25] Figure 1a shows a high-resolution transmission electron microscopy (HR-TEM) image of an FeS2 NC with a diameter of 15 ± 3 nm. The clear lattice fringes of the FeS2 NCs with a lattice spacing of 0.31 nm matched the (111) plane of pyrite. The fast Fourier transform (FFT) patterns shown in Figure 1b exhibited various index facets, including {210}, {211}, and {311} on the NC, showing typical signatures of a pyrite-phased crystal structure. Figure 1c shows a photograph of the FeS2 NCs ink. For fabricating the FeS2 NC CE, FeS2 NC ink of concentration 30 mg mL^{-1} was spin-coated onto an ITO glass substrate at 4000 rpm for 20 s, as shown in Figure 1d. Because as-

[*] Y.-C. Wang,[+] Dr. D.-Y. Wang,[+] H.-A. Chen, Prof. C.-W. Chen
Department of Materials Science and Engineering
National Taiwan University
No. 1, Sec. 4, Roosevelt Rd., Taipei, 10617 (Taiwan)
E-mail: chunwei@ntu.edu.tw

Y.-T. Jiang, Prof. C.-C. Chen
Department of Chemistry, National Taiwan Normal University
No. 162, Sec. 1, Heping East Rd., Taipei, 10610 (Taiwan)
E-mail: cjchen@ntnu.edu.tw

Prof. C.-C. Chen
Institute of Atomic and Molecular Sciences, Academia Sinica
No. 1, Sec. 4, Roosevelt Rd., Taipei, 10617 (Taiwan)

Prof. K.-C. Ho
Department of Chemical Engineering, National Taiwan University
No. 1, Sec. 4, Roosevelt Rd., Taipei, 10617 (Taiwan)

Prof. H.-L. Chou
Graduate Institute of Applied Science and Technology
National Taiwan University of Science and Technology
No.43, Sec. 4, Keelung Rd., Taipei, 10617 (Taiwan)
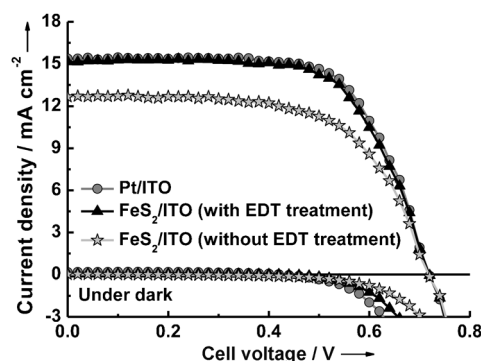
[+] These authors contributed equally to this work.

Supporting information for this article, including preparation of FeS2 nanocrystal ink, fabrication of DSCCs, characterizations, and first-principles calculations on the charge transfer and adsorption energy between I_3^- and the FeS2 NC surface, is available on the WWW under http://dx.doi.org/10.1002/anie.201300401.
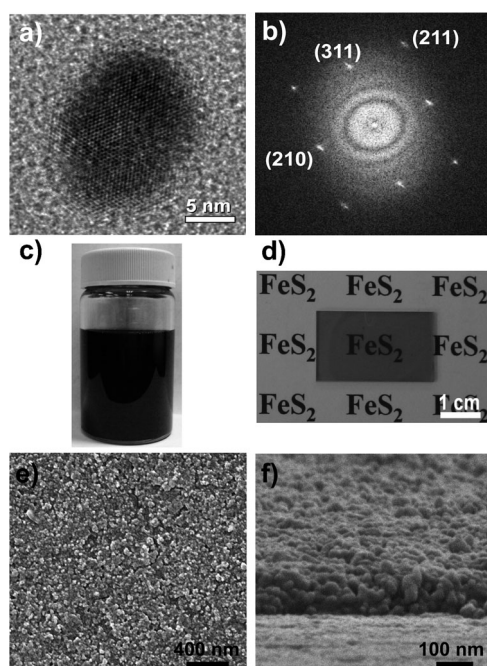
Figure 1. a) HR-TEM image and b) fast Fourier transform (FFT) pattern of FeS$_2$ NCs. c,d) Photographic images of FeS$_2$ NC ink (c) and the FeS$_2$ NC thin film (d) as a CE on the ITO glass. e,f) Top (e) and cross-sectional (f) scanning electron microscopy (SEM) images of the densely packed FeS$_2$ NC thin film on the ITO glass.

Figure 2. Current-density–voltage (*J–V*) characteristics of DSSCs with Pt-CE and FeS$_2$-CEs (with and without EDT treatment), measured in the dark and under AM 1.5 illumination (100 mW cm^{-2}).

7.31 %. The result was comparable to the performance of the reference DSSC device using the conventional Pt-CE with a J_{SC} of 15.37 mA cm^{-2}, a FF of 0.69, and an η value of 7.52 %. In contrast, the DSSC device using the FeS$_2$ NC-based CE without EDT treatment showed a lower device performance η of 5.74 % with a J_{SC} of 12.63 mA cm^{-2} and a FF of 0.64 because of the long alkyl ligands passivated on the FeS$_2$ NC surfaces. These results suggest that earth-abundant FeS$_2$ NC ink is a promising alternative to the precious Pt metal as an efficient electrocatalyst in DSSCs.

synthesized FeS$_2$ NCs are typically passivated with circa 2.5 nm long alkyl ligands (that is, oleic acid (OA) and oleylamine (OLA)), this can prevent close nanocrystal packing of FeS$_2$ thin films, thus impeding charge transport.[25,27] The FeS$_2$ NC films were subsequently dipped in 15 mM ethanedithiol (EDT) in an acetonitrile solution for 20 s and spun (at 8000 rpm for 20 s) to remove the long chain ligands from the NC surfaces and to reduce the interparticle spaces of NCs. A nearly 20-fold increase in the conductivity (5.4×10^{-3} S cm^{-1}) of the FeS$_2$ NC thin film with EDT treatment was obtained, compared to the 2.6×10^{-4} S cm^{-1} of the film without treatment.[25] Figures 1 e and f show the top and cross-sectional scanning electron microscopy (SEM) images of the densely packed FeS$_2$ NC thin film following EDT treatment with a thickness of approximately 100 nm.

Figure 2 shows the current density-voltage (*J–V*) curves of the DSSCs using FeS$_2$ NC thin films (with and without EDT treatment) and Pt as the CEs under a standard simulated AM 1.5 illumination of 100 mW cm^{-2}. The detailed parameters of the photovoltaic device performances are summarized in Table 1. These three devices showed a similar open-circuit voltage (V_{oc}) of 0.71 V. The DSSC device consisting of the EDT-treated FeS$_2$ NC thin film as a CE exhibited a short-circuit current density (J_{SC}) of 15.14 mA cm^{-2} and a fill factor (FF) of 0.68, yielding a power conversion efficiency (η) of

Table 1: Photovoltaic performance obtained from DSSCs with various CEs under AM 1.5 illumination at 100 mW cm^{-2}, parameters of EIS and Tafel polarization, and corresponding surface roughness of various CEs.

Counter electrode	V_{oc} [V]	J_{sc} [mA cm^{-2}]	FF	η [%]	R_{ct}[a] [Ω cm^2]	CPE[b] [μF]	R_{ms}[c] [nm]	J_0[d] [mA cm^{-2}]
Pt	0.71	15.37	0.69	7.52	1.47	11.67	1.36	17.45
FeS$_2$ (with EDT treatment)	0.71	15.14	0.68	7.31	1.60	38.74	10.67	16.03
FeS$_2$ (without EDT treatment)	0.71	12.63	0.64	5.74	4.54	37.21	10.28	5.66

[a] Charge-transfer resistance between the CE and the electrolyte. [b] Constant phase angle element. [c] Root-mean-square roughness. [d] Exchange current density.

Next, cyclic voltammetry (CV), electrochemical impendence spectroscopy (EIS) measurements, and Tafel curves were performed to analyze the correlation between the electrocatalytic activity of the FeS$_2$ NC CEs and the photocurrent generation. Figure 3a shows the three CVs of the devices using the reference Pt CE and FeS$_2$ NC CEs with and without EDT treatment, respectively, which consisted of a typical three-electrode device structure. Each CV curve showed two pairs of redox peaks where the redox couple at lower potential peaks (that is, between -0.4 and 0.1 V vs. Ag/Ag$^+$) corresponded to the reaction (1) of $I_3^- + 2e^- \leftrightarrow 3I^-$, and the redox couple at higher potential peaks (that is, between 0.2 and 0.6 V vs. Ag/Ag$^+$) corresponded to the reaction (2) of $3I_2 + 2e^- \leftrightarrow 2I_3^-$.[28] According to the reaction (1), the CV curve showed an anodic peak current density (J_{pa1}) and a cathodic peak current density (J_{pc1}) at the left pair of redox peaks, corresponding to the oxidation of the I^- ions and the reduction of the I_3^- ions, respectively. For the FeS$_2$ NC CE

a)

b)
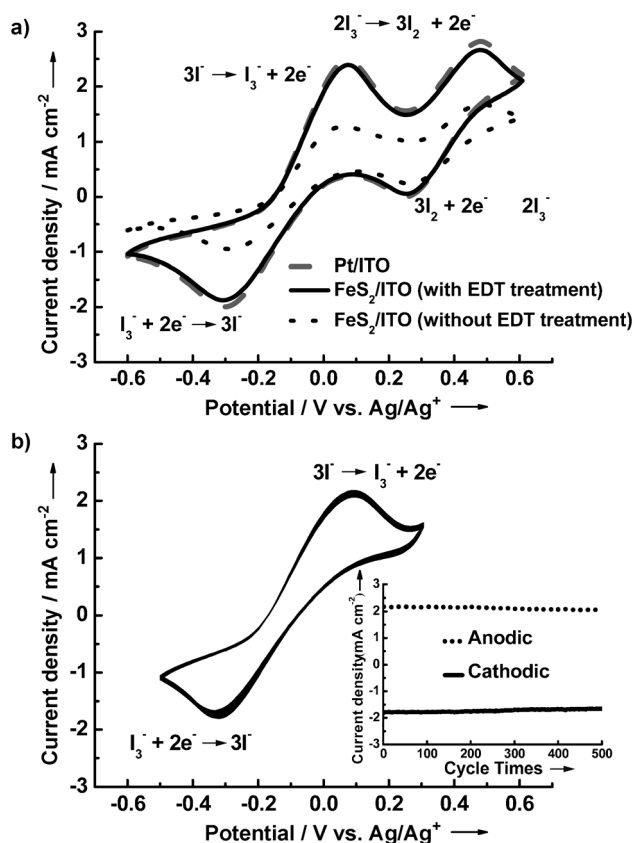
Figure 3. a) Cyclic voltammograms (CVs) of Pt-CE, FeS$_2$-CEs with and without EDT treatment, in 10 mm LiI, 1 mm I$_2$, and 0.1 m LiClO$_4$ in MeCN, at a scan rate of 50 mVs^{-1}. b) 500 consecutive CVs of FeS$_2$-CE with EDT treatment at a scan rate of 50 mVs^{-1}. Inset: anodic and cathodic peak current densities versus cycle times.

with EDT treatment, the CV profile and J_{pc1} were similar to those of the Pt CE counterpart, indicating that FeS$_2$ NCs are as effective as Pt in catalyzing the reduction of triiodide to iodide. In contrast, the magnitude J_{pc1} of the device using FeS$_2$ CE without EDT treatment was much lower compared to that of the FeS$_2$ CE with treatment. Figure 3b shows the CV profile curves and the corresponding J_{pa1} and J_{pc1} of the device using the FeS$_2$ CE with EDT treatment following 500 consecutive cycle scans. The nearly unaltered curve shape and nearly constant peak current density demonstrated the excellent electrochemical stability of the FeS$_2$ CE in the I$^-$/I$_3^-$-based electrolyte.

Figure 4a shows the Nyquist plots of the devices from the EIS measurement. The devices consisted of a symmetric sandwich-like structure (that is, CE/electrolyte/CE) fabricated using FeS$_2$ NCs and Pt electrodes, where two identical electrodes were separated between an ionomer resin spacer (Surlyn, SX1170-25). The charge transfer resistance R_{ct} was obtained by fitting the semicircle in the high-frequency region (leftmost semicircle), which corresponded to the charge-transfer process at the electrolyte/electrode interfaces, and the right-hand semicircle in the low-frequency range indicated the Nernst diffusion impedance within the electrolyte.[10,29] The charge-transfer resistance R_{ct} for the FeS$_2$ NCs with EDT treatment was 1.60 Ω cm^2, which was close to that

a)

b)
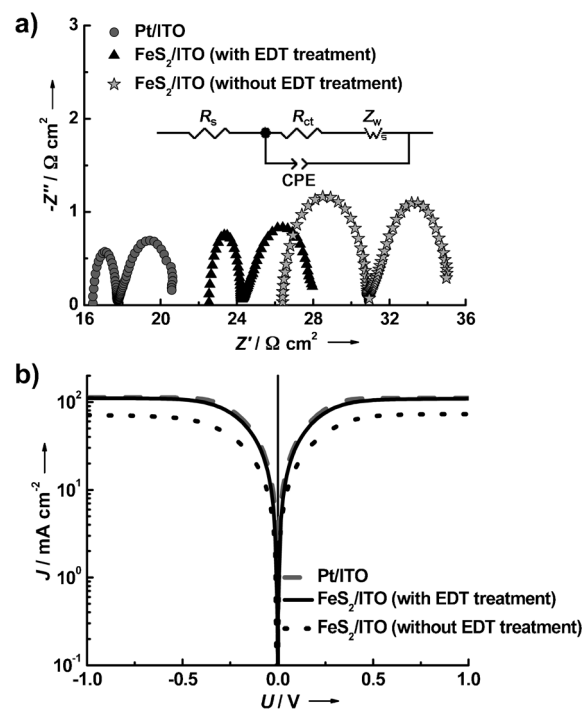
Figure 4. a) Nyquist plots of the symmetrical cells based on Pt-CE and FeS$_2$-CEs with and without EDT treatment. The frequency scan range was set from 1 MHz to 10 mHz. b) Tafel polarization curves at the scan rate of 50 mVs^{-1} based on the same devices as in (a).

of the reference Pt electrode (1.47 Ω cm^2), indicating that FeS$_2$ NCs have excellent catalytic activity. The increased R_{ct} value for the FeS$_2$ NC device without EDT treatment was attributed to the long alkyl ligands on the NC surface, which may have impeded the charge transfer rate. The corresponding constant phase-angle element (CPE) values for the FeS$_2$ CE with and without EDT treatment were 38.74 and 37.21 μF, respectively, which were significantly higher than that of the Pt CE with a CPE value of 11.67 μF, which is presumably due to the increased electrochemically active areas of the FeS$_2$ NC CEs with large surface roughness.[30] The root-mean-square roughness (R_{ms}) values determined from atomic force microscope (AFM) topography images were 1.36 nm (Pt), 10.67 nm (FeS$_2$ NC with EDT treatment), and 10.28 nm (FeS$_2$ NC without EDT treatment), as shown in the Supporting Information, Figure S2. The exchange current density (J_0), which is equal to $J_0 = RT/nFR_{ct}$,[16,31] is directly related to the electrochemical catalytic activity of the electrode, where R is the gas constant, T is the absolute temperature in K, n is number of electrons involved in the electrochemical reduction reaction, F is the Faraday constant, and R_{ct} is the charge transfer resistance. Consequently, the exchange current densities (J_0) obtained from these impendence spectroscopy data were 17.45, 16.03, and 5.66 mA cm^{-2} for the Pt CE and FeS$_2$ NC CEs with and without EDT treatment, respectively. Figure 4b shows the Tafel polarization measurement of the logarithmic current density (log$J$) as a function of voltage (U) for the oxidation/reduction of the I$^-$/I$_3^-$ redox couple with a similar device structure to that used in the Nyquist plot measurement. The exchange current densities (J_0), which can

be estimated from the extrapolated intercepts of the cathodic branches of the corresponding Tafel plots,[31] were in the consistent order of Pt > FeS$_2$ NC (with EDT treatment) > FeS$_2$ NC (without EDT treatment). Furthermore, the limiting current density J_{lim}, which was determined by the diffusion of ionic carriers between the two electrodes, was directly proportional to the diffusion coefficient (D) of the triiodide species. The J_{lim} value of the device using the FeS$_2$ NC (with EDT treatment) electrodes was similar to that using Pt. All of the CV, EIS, and Tafel polarization measurement results showed good consistency with the corresponding photovoltaic performances of DSSC devices using various CE electrodes.

Along with replacing Pt as a low-cost CE material, solution-processable FeS$_2$ NC ink has the advantage that it can be printed onto various substrates which are heat sensitive or flexible for large-area roll-to-roll production. Figure 5a shows the device performance of the DSSC with a flexible CE using the FeS$_2$ NCs ink cast onto an ITO/PET substrate. The device exhibited a power conversion efficiency (η) of 6.36% with a short-circuit current density (J_{SC}) of 14.93 mA cm^{-2}, an open-circuit voltage (V_{oc}) of 0.71 V, and a fill factor (FF) of 0.60 (under AM 1.5 illumination at

100 mW cm^{-2}). Furthermore, the semi-transparency of the FeS$_2$ NC-based CE enabled the fabrication of a bifacially active DSSC (Supporting Information, Figure S4b), which had the advantage of harvesting incident light from both sides (that is, front or rear sides). The inset of Figure 5b shows the transmission spectrum of the semi-transparent FeS$_2$ NC-based CE that had a transmittance of 50–70% ranging from 300 to 800 nm compared to that of nearly 15% for the reference Pt CE with low transparency and high reflectivity. Figure 5b shows the current-density–voltage characteristics of the DSSCs using the FeS$_2$ NC and Pt CEs as illuminated from the rear side. The DSSC device consisting of the FeS$_2$ NC CE exhibited an efficiency of 4.17%, which was approximately 57% of that from the front illumination. In contrast, the reference device using the opaque Pt-CE, as illuminated from the rear side, only had an efficiency of 1.06%. These results suggest the potential application of FeS$_2$ NC-based semi-transparent DSSCs in bifacial photovoltaic devices because of their capabilities for utilizing incident light from both sides to further reduce the cost of energy production.

In summary, this study demonstrated that FeS$_2$ NC ink is a promising alternative to the expensive Pt CE and exhibits excellent electrochemical catalytic activity and remarkable stability in catalyzing the reduction of triiodide to iodide in DSSCs. Solution-processable and semi-transparent FeS$_2$ NC-based CEs also enable the fabrication of flexible or bifacial DSSCs. The breakthrough of using earth-abundant FeS$_2$ NC ink to replace the precious metal Pt as a low-cost CE material may foster development to further bring down the cost of energy production in DSSCs. The results have also tremendous implications for future development in the low-cost nanoscale Fe-based electrocatalysts.
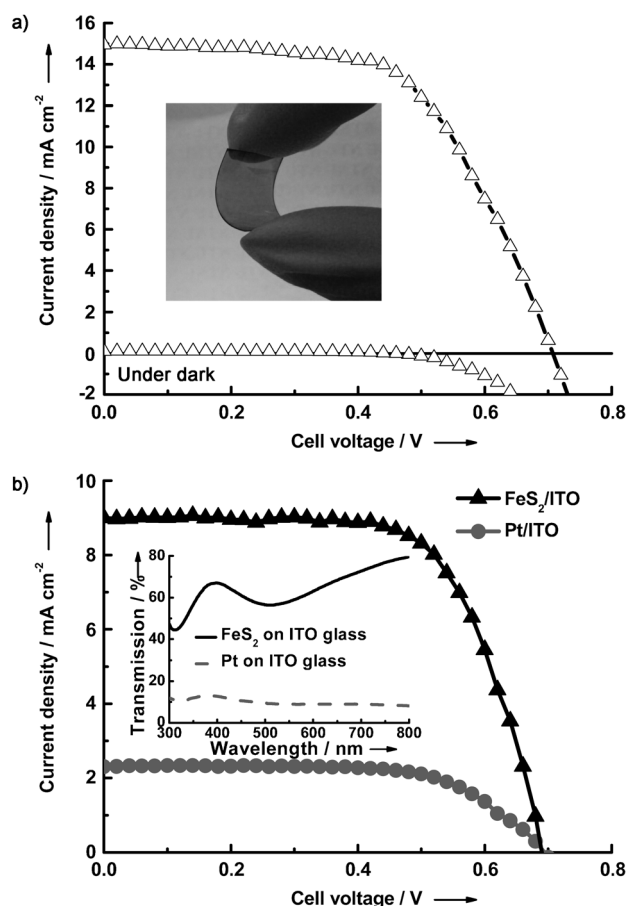
Figure 5. Current-density–voltage (J–V) characteristics of a) the DSSC using the FeS$_2$-CE deposited on ITO/PET substrate, measured in the dark and under 100 mW cm^{-2} illumination; b) DSSCs consisting of the reference Pt-CE and semi-transparent FeS$_2$-CE under rear illumination (100 mW cm^{-2}). Inset: the corresponding transmittance of Pt-CE and FeS$_2$-CE.

[1] O. Reagan, M. Grätzel, *Nature* **1991**, *353*, 737–740.
[2] M. Grätzel, *Nature* **2001**, *414*, 338–344.
[3] A. I. Hochbaum, P. Yang, *Chem. Rev.* **2010**, *110*, 527–546.
[4] A. Yella, H. W. Lee, H. N. Tsao, C. Yi, A. K. Chandiran, M. Na, M. K. Nazeeruddin, E. W. G. Diau, C. Y. Yeh, S. M. Zakeeruddin, M. Grätzel, *Science* **2011**, *334*, 629–634.
[5] B. E. Hardin, H. J. Snaith, M. D. McGehee, *Nat. Photonics* **2012**, *6*, 162–169.
[6] G. Boschloo, A. Hagfeldt, *Acc. Chem. Res.* **2009**, *42*, 1819–1826.
[7] Y. Xu, H. Bai, G. Lu, C. Li, G. Shi, *J. Am. Chem. Soc.* **2008**, *130*, 5856–5857.
[8] J. D. Roy-Mayhew, D. J. Bozym, C. Punckt, I. A. Aksay, *ACS Nano* **2010**, *4*, 6203–6211.
[9] L. J. Brennan, M. T. Byrne, M. Bari, Y. K. Gun'ko, *Adv. Energy Mater.* **2011**, *1*, 472–485.
[10] S. Das, P. Sudhagar, V. Verma, D. Song, E. Ito, S. Y. Lee, Y. S. Kang, W. Choi, *Adv. Funct. Mater.* **2011**, *21*, 3729–3736.
[11] J. Xia, L. Chen, S. Yanagida, *J. Mater. Chem.* **2011**, *21*, 4644–4649.
[12] Y. Xue, J. Liu, H. Chen, R. Wang, D. Li, J. Qu, L. Dai, *Angew. Chem.* **2012**, *124*, 12290–12293; *Angew. Chem. Int. Ed.* **2012**, *51*, 12124–12127.

[13] M. Wu, X. Lin, A. Hagfeldt, T. Ma, *Angew. Chem.* **2011**, *123*, 3582–3586; *Angew. Chem. Int. Ed.* **2011**, *50*, 3520–3524.

[14] X. Xin, M. He, W. Han, J. Jung, Z. Lin, *Angew. Chem.* **2011**, *123*, 11943–11946; *Angew. Chem. Int. Ed.* **2011**, *50*, 11739–11742.

[15] Y. Hu, Z. Zheng, H. Jia, Y. Tang, L. Zhang, *J. Phys. Chem. C* **2008**, *112*, 13037–13042.

[16] M. Wang, A. M. Anghel, B. Marsan, N. L. C. Ha, N. Pootrakul- chote, S. M. Zakeeruddin, M. Grätzel, *J. Am. Chem. Soc.* **2009**, *131*, 15976–15977.

[17] G. R. Li, F. Wang, Q. W. Jiang, X. P. Gao, P. W. Shen, *Angew. Chem.* **2010**, *122*, 3735–3738; *Angew. Chem. Int. Ed.* **2010**, *49*, 3653–3656.

[18] H. Sun, D. Qin, S. Huang, X. Guo, D. Li, Y. Luo, Q. Meng, *Energy Environ. Sci.* **2011**, *4*, 2630–2637.

[19] M. Wu, X. Lin, Y. Wang, L. Wang, W. Guo, D. Qi, X. Peng, A. Hagfeldt, M. Grätzel, T. Ma, *J. Am. Chem. Soc.* **2012**, *134*, 3419–3428.

[20] C. W. Kung, H. W. Chen, C. Y. Lin, K. C. Huang, R. Vittal, K. C. Ho, *ACS Nano* **2012**, *6*, 7016–7025.

[21] C. Wadia, A. P. Alivisatos, D. M. Kammen, *Environ. Sci. Technol.* **2009**, *43*, 2072–2077.

[22] Y. Y. Lin, D. Y. Wang, H. C. Yen, H. L. Chen, C. C. Chen, C. M. Chen, C. Y. Tang, C. W. Chen, *Nanotechnology* **2009**, *20*, 405207.

[23] J. Puthussery, S. Seefeld, N. Berry, M. Gibbs, M. Law, *J. Am. Chem. Soc.* **2011**, *133*, 716–719.

[24] Y. Bi, Y. B. Yuan, C. L. Exstrom, S. A. Darveau, J. S. Huang, *Nano Lett.* **2011**, *11*, 4953–4957.

[25] D. Y. Wang, Y. T. Jiang, C. C. Lin, S. S. Li, Y. T. Wang, C. C. Chen, C. W. Chen, *Adv. Mater.* **2012**, *24*, 3415–3420.

[26] M. A. Hines, G. D. Scholes, *Adv. Mater.* **2003**, *15*, 1844–1849.

[27] E. J. D. Klem, H. Shukla, S. Hinds, D. D. MacNeil, L. Levina, E. H. Sargent, *Appl. Phys. Lett.* **2008**, *92*, 212105.

[28] A. I. Popov, D. H. Geske, *J. Am. Chem. Soc.* **1958**, *80*, 1340–1352.

[29] F. Fabregat-Santiago, J. Bisquert, E. Palomares, L. Otero, D. B. Kuang, S. M. Zakeeruddin, M. Grätzel, *J. Phys. Chem. C* **2007**, *111*, 6550–6560.

[30] M. Wu, X. Lin, A. Hagfeldt, T. Ma, *Chem. Commun.* **2011**, *47*, 4535–4537.

[31] A. J. Bard, L. R. Faulkner, *Electrochemical methods: fundamen- tals and applications*, second edition, Wiley, New York, **2001**, pp. 93–105.